RSC Advances

PAPER

Published on 28 October 2026
Licensed under CC-BY-NC 4.0

Check for updates

Cite this: DOI: 10.1039/d6ra08114b

First hyperpolarizability of dithienylethene-based photoswitches: a structure–property relationship study

Kanchan Sarkar, [a] Ramprasad Misra, *[b] Axel Groß [a] and Rudraditya Sarkar *[c]

Despite their considerable technological potential, structure–property relationships in intramolecular charge-transfer-based photoswitches remain poorly established. Here, we present a quantum-chemical investigation of the first hyperpolarizability (β) of a family of dithienylethene (DTE)-based photoswitches, considering static, electro-optic Pockels, and second-harmonic-generation (SHG) responses. Eight donor (D)/acceptor (A) architectures, with and without alkyne (y) π-extension, are investigated in their open- and closed-ring forms using density functional theory [CAM-B3LYP/6-31+G(d,p)/GD3BJ/(PCM)] in the gas phase and three continuum solvents, with dynamic responses evaluated at 1064 nm. Ring closure generally enhances total first hyperpolarizability (β_{tot}) by restoring through core conjugation, while donor–acceptor asymmetry emerges as the dominant structural factor governing large NLO responses. Alkyne extension further enhances the response when coupled with a push–pull architecture. Solvation modulates both the magnitude and direction of the response, producing pronounced amplification of the closed/open β_{tot} ratio in selected systems and a striking reorientation of the SHG response vector for Dy–yA$_{open}$. Time-dependent DFT analysis suggests that the reorientation is associated with a redistribution among nearby excited-state contribution. Importantly, β_{tot} and the directional alignment ratio η are not necessarily correlated. We therefore introduce R_{NLO} as a combined comparative descriptor that captures both response magnitude and directionality. R_{NLO} identifies the closed push–pull architectures, particularly Dy–yA$_{closed}$, D–yA$_{closed}$, and Dy–A$_{closed}$, as the most favorable systems among the considered chromophores. Overall, the results show that NLO performance is governed by the coupled effects of donor–acceptor asymmetry, ring closure, π-extension, and dielectric environment, and that optimization of both response magnitude and directionality is essential for establishing meaningful structure–property relationships in DTE photoswitches.

Received 28th August 2026
Accepted 18th October 2026

DOI: 10.1039/d6ra08114b

rsc.li/rsc-advances

1 Introduction

Second-order nonlinear optical (NLO) processes are central to modern photonics. Second-harmonic generation (SHG) and frequency mixing drive electro-optic modulation to the integrated and on-chip light sources,[1] which enables their high-speed optical communication.[2] Harmonic generation (such as second- and third-harmonic generation) is extensively investigated in molecular, organic, and low-dimensional materials[3] because these materials can exhibit strong nonlinear optical responses. At the molecular level, the relevant quantity is the first hyperpolarizability β, a third-rank tensor that links the induced dipole to the second power of the applied electric field.[4,5] The size of the tensor by itself is not enough to determine the strength of the NLO responses, sometimes a large tensor can still give a weak measurable response if it points the wrong way relative to the permanent molecular dipole. Therefore, it is necessary to treat the direction of the response as a property in its own right, alongside its size. The magnitude and direction of the first hyperpolarizability can be optimized through molecular design, achieving dynamic control over these properties remains a significant challenge. This motivates the exploration of molecular systems whose nonlinear optical response can be reversibly modulated by external stimuli, particularly light. In this regard, donor–acceptor (D–A) chromophores are a common molecular design motif for large second-order responses.[6–9] Intramolecular charge transfer (ICT) breaks inversion symmetry and creates a polarizable pathway along the donor–acceptor axis. Extending the conjugated linker in a D–π–A architecture often increases the static response,[10,11] and chemical tuning through the electronic donor, acceptor and π-conjugation bridge is well

[a]Institut für Theoretische Chemie, Universität Ulm, Oberberghof 7, 89081 Ulm, Germany

[b]Institut für Biologie, Humboldt-Universität zu Berlin, Invalidenstraße 42, 10115 Berlin, Germany. E-mail: ramprasad.misra@hu-berlin.de

[c]Department of Chemistry, GITAM School of Science, Hyderabad 502329, Telangana, India. E-mail: rudra.smgr@gmail.com; rsarkar2@gitam.edu

© 2026 The Author(s). Published by the Royal Society of Chemistry

studied.[12–14] Once a molecule has been designed, its functional response is generally fixed by its molecular structure. A compelling question is whether a single molecular framework can be engineered to exhibit two distinct responses and be reversibly switched between them using light. Photoisomerizable scaffolds address this question directly. Illumination can alter conjugation and electronic connectivity without changing the molecular formula. This principle underlies a broad family of molecular switches and motors,[15,16] including systems whose photochromism reconfigures emission or charge-transfer character,[17] and the NLO response itself can be switched in this way.[18,19] Dithienylethenes (DTEs) are particularly well suited for such a comparison,[20–23] and donor–acceptor diarylethenes have been developed specifically for NLO and near-infrared photochromic applications.[19,24–27] Their open and closed forms differ in the connectivity through the central hexatriene/cyclohexadiene unit, so ring closure changes the conjugated path that links the two thiophene-substituent arms. Recently, Anderson and co-workers[28] reported a structurally consistent DTE photoswitches in which a julolidine donor (D), an *N*-methylpyridinium acceptor (A), and an alkyne extension (denoted *y*) are varied systematically.

In the present work we set to study the series of DTE molecules (Fig. 1) synthesized by Anderson and co-workers[28] as a model system to examine how the calculated static, electro-optic Pockels, and SHG first hyperpolarizability tensors vary across the open and closed DTE architectures. It is noted that the experimental chromophores[28] are isolated as PF_6- salts, while present calculations consider those as counterion-free molecular ions (elaborately discussed in the Computational methods section). The series of chromophores (Fig. 1) studied in this work gives us systematically varied experimental series[28] for separating the effects of ring state, donor–acceptor asymmetry, alkyne extension, and continuum solvation on the calculated NLO tensor. We analyze the tensor norm β_{tot}, the projection of the response along the permanent dipole β_{vec}, and the alignment ratio $\eta = \beta_{vec}/\beta_{tot}$ together.[29] We also avoid using the HOMO–LUMO gap as a stand-alone predictor of resonant response as near-resonant denominators, transition-dipole couplings, solvent stabilization, and tensor-component interference can change the magnitude and sign of β in ways that a single orbital gap cannot account for.[29–32]

2 Computational and theoretical details

2.1 Geometry optimizations and electronic structure

All ground-state geometries were optimized using density functional theory (DFT) with the long-range-corrected hybrid functional CAM-B3LYP[33] and the 6-31+G(d,p) basis set.[34] Long-range correction is appropriate for ICT-based chromophores,[35] where standard hybrid functionals underestimate excitation energies of charge-transfer states.[36,37] The total charge of the considered chromophores varies across the series, D–D and D*y*–*y*D are neutral; the asymmetric push–pull motifs D–A, D*y*–A, D–*y*A and D*y*–*y*A are monocations (charge +1, owing to the cationic *N*-methylpyridinium acceptor); A–A and A*y*–*y*A are dications (charge +2). The PF_6^- counterions present in the experimental[28] acceptor salts were not included. This counterion-free model was chosen to isolate the chromophore-intrinsic topology effects that are the subject of the study and to keep comparisons across the series internally consistent. Explicit ion pairing and counterion local-field effects may shift absolute β values, particularly in low-dielectric environments, and are outside the scope of the present study. Solvent effects on geometries and properties were modeled using the self-consistent reaction field (SCRF) polarizable-continuum model[38,39] for three solvent media spanning $\varepsilon \approx 10$–36, dichloroethane (DCE, $\varepsilon = 10.13$), 1-nitropropane (NP, $\varepsilon = 23.73$), and acetonitrile (ACN, $\varepsilon = 35.69$) using Gaussian 16 program module.[40] The open- and closed-ring isomer of each chromophore was optimized independently in each medium and then used that optimized structure as the reference geometry for the corresponding response calculations. The optimized structures of the chromophores in ACN are shown in Fig. 2. The response calculations were performed with the same DFT functional and basis set, augmented with Grimme's empirical dispersion correction with Becke–

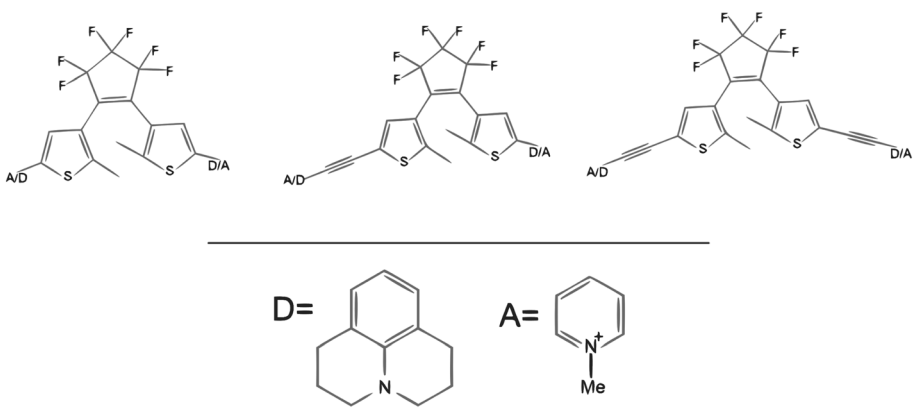


Fig. 1 Dithienylethene-based molecules/photoswitches considered in this work. Eight DTE motifs are studied, separating the effects of julolidine donor (D) substitution, *N*-methylpyridinium acceptor (A) substitution, alkyne extension (*y*), and the open/closed ring isomeric state. The syntheses of these molecules are reported by Anderson and co-workers.[28]

© 2026 The Author(s). Published by the Royal Society of Chemistry

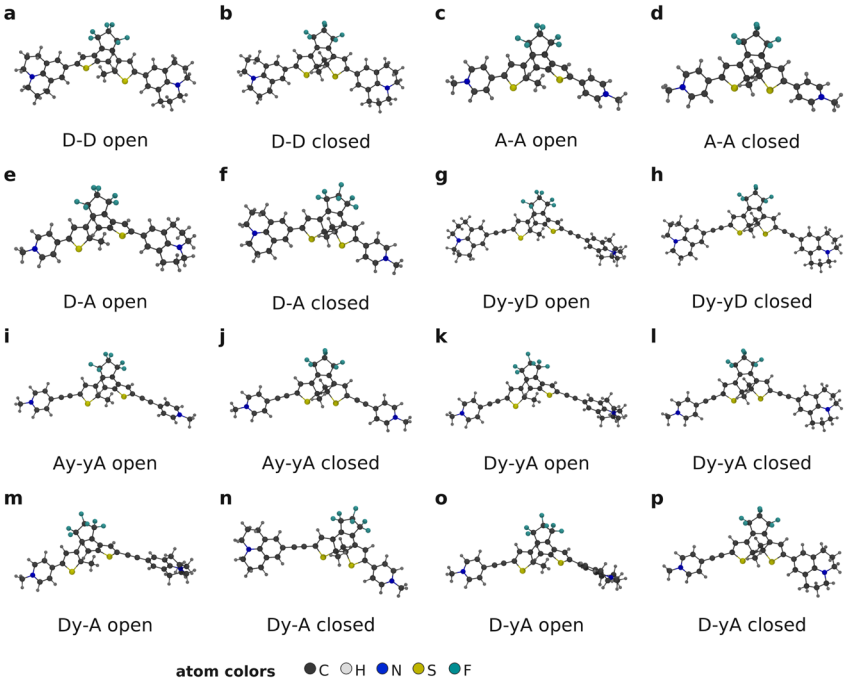


Fig. 2 Optimized structures of the open- and closed-ring forms of the studied chromophores in acetonitrile, obtained at the CAM-B3LYP/6-31+G(d,p) level of theory with a polarizable continuum description of the solvent.

Johnson damping (GD3BJ).[41] Frontier orbitals, HOMO–LUMO gaps, and electron-density-difference (EDD) maps were computed at the optimized acetonitrile structures. The EDD maps shown in Fig. 3 and 4 report the change in electron density associated with the dominant HOMO → LUMO single-orbital transition, with the same isosurface threshold across all panels. To probe the solvent-induced 2P response-vector re-orientation of D*y*–*y*A_{open}, additional time-dependent density functional theory (TDDFT) vertical excitations were computed for the gas-phase and acetonitrile geometries at the same CAM-B3LYP/6-31+G(d,p) level with Grimme's empirical dispersion correction. These calculations include the estimation of the lowest five singlet excitation energies, oscillator strengths, dominant orbital-transition characters, and ground-to-excited transition-dipole components. Frequency-dependent calculations were performed at $\omega = 0.0428$ a.u., which corresponds to a perturbation wavelength of approximately 1064 nm, commonly provided by an Nd:YAG laser for molecular SHG measurements.[42] The present calculations report frequency-dependent NLO properties in two different regimes, (i) one-photon (1P) response or Pockels effect[29] corresponds to linear electro-optic hyperpolarizability $\beta(-\omega; \omega, 0)$ and (ii) two-photon (2P) response corresponds to the second-harmonic-generation (SHG) hyperpolarizability $\beta(-2\omega; \omega, \omega)$. The computed Pockels and SHG hyperpolarizabilities are summarized in Tables S5–S12. All quantum-chemical calculations were performed using the Gaussian 16 quantum chemical package.[40] Geometries, orbitals, and density-difference surfaces were visualized from Gaussian 16 formatted-checkpoint and cube files using GaussView 6 [43] visualization software.

2.2 Hyperpolarizability tensor and structure–property descriptors

The first hyperpolarizability β is a third-rank tensor with twenty-seven components, applying Kleinman intrinsic-permutation symmetry[44] reduces the tensor elements from twenty-seven to ten independent elements for the static response, which are β_{xxx}, β_{xxy}, β_{xxz}, β_{xyy}, β_{xyz}, β_{xzz}, β_{yyy}, β_{yyz}, β_{yzz} and β_{zzz}. Static β was evaluated by analytic coupled-perturbed Kohn–Sham response,[45] and the frequency-dependent $\beta(-\omega; \omega, 0)$ and $\beta(-2\omega; \omega, \omega)$ tensors by the corresponding time-dependent linear-response procedure as implemented in Gaussian 16.[40] The components of the β can be calculated using the following equation

$$\beta_i = \beta_{iii} + \frac{1}{3}\sum_{j\neq i}\left(\beta_{ijj} + \beta_{jij} + \beta_{jji}\right), \quad i = x, y, z. \tag{1}$$

The magnitude of the total dipole moment (μ) and average polarizability (α_{av}) and total first hyperpolarizability (β_{tot})[46] within the *xyz* coordinate representation can be calculated using equations given in eqn (2),

$$\begin{aligned} \mu &= \sqrt{\mu_x{}^2 + \mu_y{}^2 + \mu_z{}^2}, \\ \alpha_{av} &= \frac{1}{3}\left(\alpha_{xx} + \alpha_{yy} + \alpha_{zz}\right), \\ \beta_{tot} &= \sqrt{\beta_x{}^2 + \beta_y{}^2 + \beta_z{}^2}, \end{aligned} \tag{2}$$

while the complete equation to calculate the β_{tot} from the Gaussian-16 (ref. 40) outputs is given in eqn (3).

© 2026 The Author(s). Published by the Royal Society of Chemistry

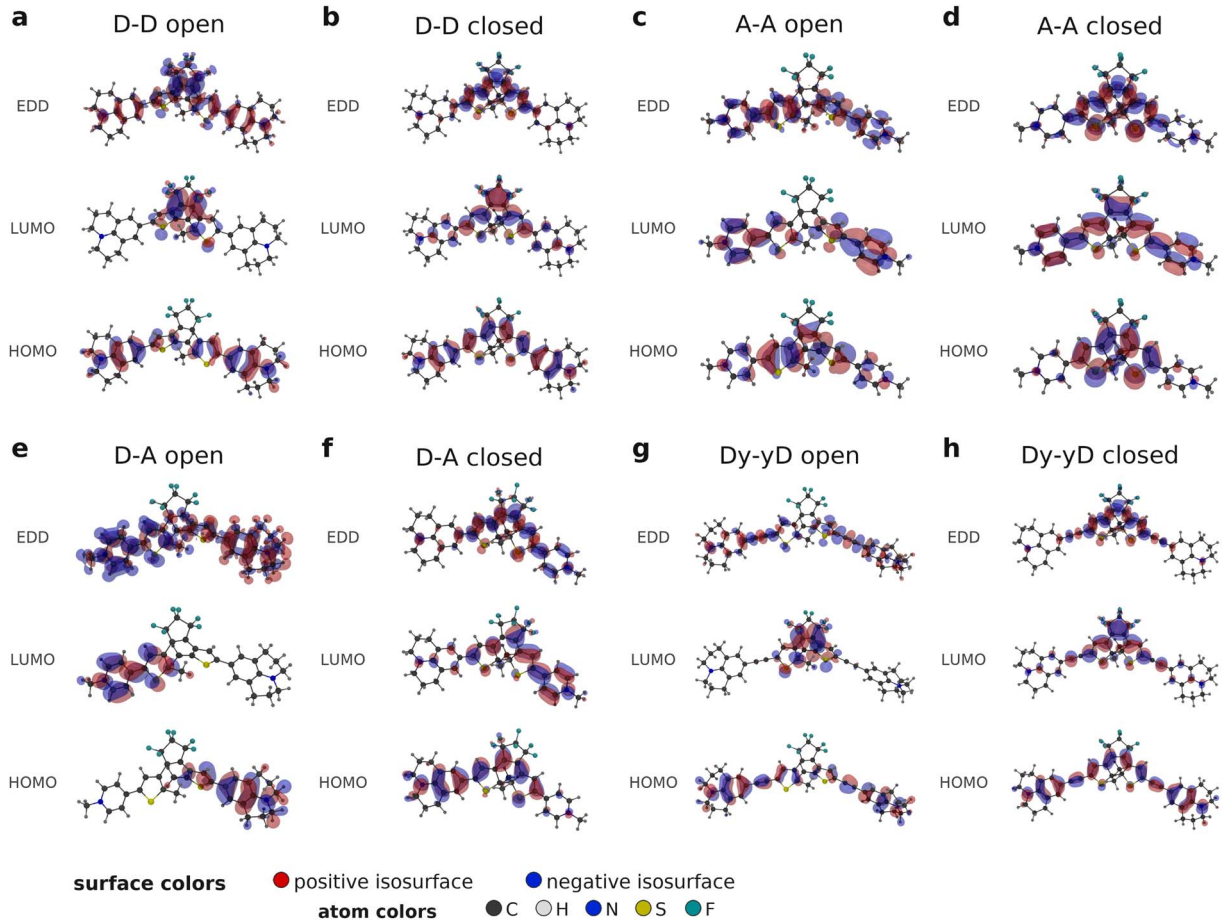


Fig. 3 HOMO and LUMO frontier orbitals and the corresponding HOMO → LUMO electron-density-difference (EDD) maps for the open- and closed-ring forms of D–D, A–A, D–A, and D*y*–*y*D, optimized in acetonitrile. The isovalue used for MO plots is 0.02, while the isovalue for density plots is 0.0004. Red (positive) lobes correspond to density accumulation and blue (negative) lobes correspond to density depletion upon the HOMO-to-LUMO single-orbital transition.

$$\beta_{tot} = [(\beta_{xxx} + \beta_{xyy} + \beta_{xzz})^2 + (\beta_{xxy} + \beta_{yyy} + \beta_{yzz})^2 + (\beta_{xxz} + \beta_{yyz} + \beta_{zzz})^2]^{1/2}. \quad (3)$$

The vector component of the first hyperpolarizability (β_{vec}) is defined in eqn (4), while a dimensionless alignment ratio[47] (η) used throughout the study is defined in eqn (5)

$$\beta_{vec} = \sum_i \frac{\beta_i \mu_i}{|\boldsymbol{\mu}|}, \quad i = x, y, z, \quad (4)$$

$$\eta = \frac{\beta_{vec}}{\beta_{tot}}. \quad (5)$$

The calculated μ and α_{av} values in gas phase and different solvent medium are given in Tables S1–S8, while the components of β, β_{tot}, β_{vec} and η calculated in gas phase and in different solvent medium are tabulated in Tables S1–S12. The tabulated tensor components are reported in a frame whose z axis lies along the permanent dipole, so that the z component of β_{vec}, that is, β_z in eqn (4) lies along the permanent dipole and β_x, β_y components are transverse to the dipole. Geometrically, η is the cosine of the angle between the response vector (β_x, β_y, β_z) and the molecular dipole $\boldsymbol{\mu}$.[47] Values $|\eta| \rightarrow 1$ indicate that the response vector is collinear with the molecular dipole (with the sign giving the sense of the response relative to the chosen dipole orientation), whereas $|\eta| \ll 1$ signals tensor cancellation or competing response directions.[29,47]

As discussed in the following sections, a meaningful structure–property relationship for the NLOPs of the investigated chromophores cannot be established using either β_{tot} or η, alone. This is because these two descriptors characterize different aspects of the NLO response and are not linearly correlated. Specifically, β_{tot} represents the magnitude of the first hyperpolarizability, whereas η describes its directional character. Consequently, consideration of either descriptor individually provides only a partial representation of the NLO response. A combined descriptor that simultaneously incorporates both the magnitude and directional characteristics is therefore desirable.

To construct such a descriptor, we first normalized β_{tot} over the entire chromophore data set using its minimum ($|\beta_{tot}|_{min}$) and maximum ($|\beta_{tot}|_{max}$) values on a logarithmic scale. The

© 2026 The Author(s). Published by the Royal Society of Chemistry

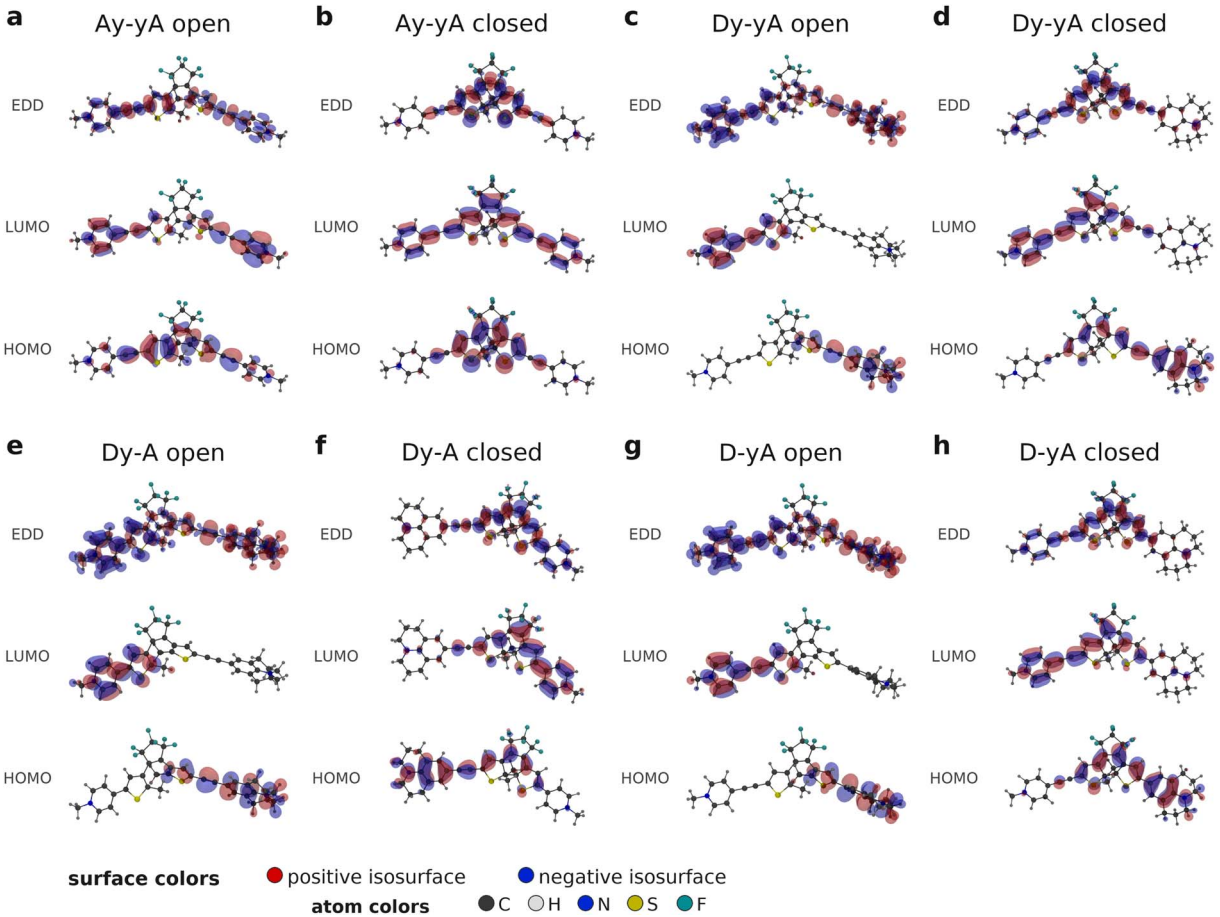


Fig. 4 HOMO and LUMO frontier orbitals and the corresponding HOMO → LUMO EDD maps for the open- and closed-ring forms of A*y*–*y*A, D*y*–*y*A, D*y*–A, and D–*y*A in acetonitrile. The push–pull alkyne-extended systems (D*y*–*y*A in particular) show the strongest end-to-end charge-transfer character upon ring closure. MO and EDD maps use the same common isosurface threshold as Fig. 3.

logarithmic normalization was employed to accommodate the large dynamic range of the hyperpolarizability values. The resulting dimensionless quantity, β_{norm}, is defined as

$$\beta_{\mathrm{norm}} = \frac{\log|\beta_{\mathrm{tot}}| - \log|\beta_{\mathrm{tot}}|_{\mathrm{min}}}{\log|\beta_{\mathrm{tot}}|_{\mathrm{max}} - \log|\beta_{\mathrm{tot}}|_{\mathrm{min}}}. \quad (6)$$

Thus, β_{norm} provides a dimensionless measure of the relative magnitude of the hyperpolarizability within the investigated chromophore series, with values ranging from 0 to 1, corresponding to the minimum and maximum β_{tot}, respectively.

Subsequently, we introduce a combined molecular descriptor, R_{NLO}, defined as

$$R_{\mathrm{NLO}} = \beta_{\mathrm{norm}}\eta,. \quad (7)$$

By combining the normalized magnitude of the hyperpolarizability with its directional contribution, R_{NLO} provides a single dimensionless descriptor that simultaneously captures how large the NLO response is and how strongly it is directionally expressed. Therefore, R_{NLO} is expected to provide a comprehensive basis for establishing structure–property relationships across the investigated chromophores.

3 Results and discussion

The optimized structures of the open- and closed-ring forms of the studied chromophores in acetonitrile are shown in Fig. 2. The results are presented as follows: the frontier-orbital reorganization upon ring closure is reported first, followed by the static β. Then, the frequency and solvent dependence on the β are presented, and finally the structure–property relationships are discussed.

3.1 Frontier-orbital reorganization upon ring closure

The HOMO/LUMO and EDD plots in Fig. 3 and 4 show that ring closure restores a continuous conjugation path through the DTE core and thereby sets whether the electronic response can be directed. In the open form of every chromophore, the central hexatriene unit interrupts the conjugated pathway between the two thiophene-substituent arms, so frontier orbitals are largely localized on one or the other side. Ring closure converts this interrupted pathway into a continuous one. In the symmetric D–D, A–A, D*y*–*y*D and A*y*–*y*A scaffolds the response grows but stays symmetric and the overall polarization is small as one finds less delocalization of the respective EDD plots (*cf.* panels

© 2026 The Author(s). Published by the Royal Society of Chemistry

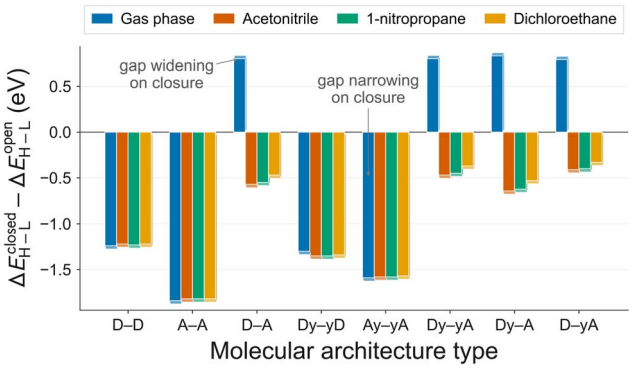


Fig. 5 HOMO–LUMO gap modulation upon ring closure, reported as $\Delta E_{H-L}^{closed} - \Delta E_{H-L}^{open}$, in the gas phase and in the three continuum solvents. Negative values therefore indicate gap narrowing upon closure. In solvent, ring closure reduces the gap for every chromophore. In the gas phase, push–pull chromophores show the opposite trend, a slight widening on closure. The gap is a useful marker of conjugation extension, but it does not predict β_{tot} one-to-one, especially in the resonant regimes.

a–d, g and h in Fig. 3 and panels a and b in Fig. 4). In the donor–acceptor scaffolds, by contrast, ring closure produces a continuous polarizable bridge that connects donor and acceptor, and the redistribution of charge upon excitation becomes spatially extended along that bridge. The alkyne-extended push–pull architectures D*y*–A, D–*y*A, and especially D*y*–*y*A combine the largest end-to-end polarization with the most spatially extended charge-transfer character (*cf.* panels c and d in Fig. 4), and these are the systems that produce the largest hyperpolarizabilities. In continuum solvents, ring closure reduces the HOMO–LUMO energy gap (ΔE) in every chromophore class (*cf.* Table S13). In the gas phase this holds only for the symmetric scaffolds (D–D, A–A, D*y*–*y*D, A*y*–*y*A). For the gas-phase push–pull chromophores (D–A, D*y*–*y*A, D*y*–A, D–*y*A), the closed-form gap is, counter-intuitively, slightly larger than the open-form gap, reflecting the closed form's deeper-lying HOMO once the conjugated DTE bridge is restored (Fig. 5 and Table S13). A similar relationship between ring state and orbital energies has been reported for related diarylethene NLO switches.[19] In the simplest two-level picture, $\beta \propto \mu_{ge}^{2}\Delta E^{-3}$, where μ_{ge} is the ground-to-excited-state transition dipole.[48,49] In the gas phase, symmetric closed forms have moderate gaps (~4 eV) and modest β, while asymmetric closed forms have somewhat smaller gaps (~3 eV) and roughly an order of magnitude larger β. It is noted that the frontier-orbital analysis only provides a qualitative diagnostic of β.

To the best of our knowledge, experimental first-hyperpolarizability data are not available for this eight-member DTE series. Qiu, Anderson and co-workers[28] reported the photophysical and photochemical properties of the same molecular set, including the near-infrared absorption band of the closed push–pull DTEs at $\lambda_{max} \approx 800$ nm.[28] We compared this absorption band with the calculated lowest bright singlet energies. These occur at about 780–850 nm in the gas phase and 650–720 nm in the continuum solvents (Table S15). The gas-phase values cover the reported ~800 nm band, while the

Table 1 Total first hyperpolarizability β_{tot} (a.u., always positive) for all sixteen structures, grouped by static, 1P (Pockels), and 2P (SHG) regimes. Computed with the full frequency-dependent response vector. ‡ marks 2P symmetric-closed cells that are unstable under the zero-damping ($\Gamma = 0$) convention near 2ω

	Static				1P (Pockels)				2P (SHG)			
Molecule	Gas	ACN	NP	DCE	Gas	ACN	NP	DCE	Gas	ACN	NP	DCE
D–D$_{open}$	1.89×10^{3}	5.15×10^{3}	5.04×10^{3}	4.66×10^{3}	2.24×10^{3}	4.68×10^{3}	4.73×10^{3}	4.60×10^{3}	3.33×10^{3}	6.25×10^{3}	6.40×10^{3}	6.38×10^{3}
D–D$_{closed}$	9.00×10^{3}	3.46×10^{4}	3.37×10^{4}	3.01×10^{4}	1.29×10^{4}	3.75×10^{4}	3.81×10^{4}	3.63×10^{4}	8.73×10^{4}‡	1.38×10^{4}‡	1.24×10^{4}‡	1.31×10^{4}‡
A–A$_{open}$	1.56×10^{3}	2.94×10^{3}	2.92×10^{3}	2.87×10^{3}	1.85×10^{3}	2.80×10^{3}	2.85×10^{3}	2.92×10^{3}	2.87×10^{3}	3.89×10^{3}	4.04×10^{3}	4.23×10^{3}
A–A$_{closed}$	7.30×10^{3}	9.07×10^{3}	9.08×10^{3}	9.12×10^{3}	1.19×10^{4}	9.98×10^{3}	1.04×10^{4}	1.12×10^{4}	4.53×10^{3}‡	3.54×10^{3}‡	3.25×10^{3}‡	2.75×10^{3}‡
D–A$_{open}$	2.34×10^{4}	1.62×10^{4}	1.62×10^{4}	1.63×10^{4}	5.59×10^{4}	1.56×10^{4}	1.60×10^{4}	1.68×10^{4}	8.68×10^{3}	2.27×10^{4}	2.39×10^{4}	2.62×10^{4}
D–A$_{closed}$	4.52×10^{4}	2.54×10^{4}	2.56×10^{4}	2.62×10^{4}	4.90×10^{4}	3.61×10^{4}	3.93×10^{4}	4.66×10^{4}	2.57×10^{4}	1.11×10^{4}	1.08×10^{4}	8.55×10^{4}
Dy–yD$_{open}$	4.56×10^{3}	1.12×10^{4}	1.10×10^{4}	1.03×10^{4}	5.57×10^{3}	1.08×10^{4}	1.09×10^{4}	1.07×10^{4}	8.95×10^{3}	1.61×10^{4}	1.65×10^{4}	1.65×10^{4}
Dy–yD$_{closed}$	1.97×10^{4}	6.89×10^{4}	6.71×10^{4}	6.07×10^{4}	2.90×10^{4}	8.22×10^{4}	8.32×10^{4}	7.95×10^{4}	1.61×10^{4}‡	3.48×10^{4}‡	3.83×10^{4}‡	3.77×10^{4}‡
Ay–yA$_{open}$	5.77×10^{3}	8.84×10^{3}	8.80×10^{3}	8.77×10^{3}	7.37×10^{3}	8.75×10^{3}	8.96×10^{3}	9.30×10^{3}	1.40×10^{4}	1.37×10^{4}	1.43×10^{4}	1.53×10^{4}
Ay–yA$_{closed}$	2.11×10^{4}	1.88×10^{4}	1.89×10^{4}	1.90×10^{4}	4.02×10^{4}	2.29×10^{4}	2.40×10^{4}	2.58×10^{4}	4.54×10^{4}‡	6.15×10^{3}‡	7.30×10^{3}‡	9.69×10^{3}‡
Dy–yA$_{open}$	5.65×10^{4}	3.42×10^{4}	3.43×10^{4}	3.49×10^{4}	2.52×10^{5}	3.49×10^{4}	3.60×10^{4}	3.81×10^{4}	1.09×10^{4}	5.68×10^{4}	5.96×10^{4}	6.57×10^{4}
Dy–yA$_{closed}$	3.11×10^{5}	2.81×10^{5}	2.86×10^{5}	3.04×10^{5}	1.38×10^{6}	4.28×10^{5}	4.59×10^{5}	5.45×10^{5}	2.82×10^{7}	2.10×10^{5}	2.10×10^{5}	2.08×10^{5}
Dy–A$_{open}$	3.61×10^{4}	2.44×10^{4}	2.44×10^{4}	2.46×10^{4}	1.04×10^{5}	2.44×10^{4}	2.50×10^{4}	2.63×10^{4}	6.17×10^{3}	3.78×10^{4}	3.96×10^{4}	4.30×10^{4}
Dy–A$_{closed}$	1.45×10^{5}	2.85×10^{5}	2.90×10^{5}	3.09×10^{5}	3.76×10^{5}	4.22×10^{5}	4.56×10^{5}	5.50×10^{5}	1.79×10^{6}	1.10×10^{5}	1.04×10^{5}	9.26×10^{4}
D–yA$_{open}$	3.99×10^{4}	2.63×10^{4}	2.65×10^{4}	2.73×10^{4}	1.13×10^{5}	2.63×10^{4}	2.72×10^{4}	2.93×10^{4}	2.54×10^{4}	4.17×10^{4}	4.40×10^{4}	4.95×10^{4}
D–yA$_{closed}$	1.43×10^{5}	2.74×10^{5}	2.78×10^{5}	2.93×10^{5}	4.36×10^{5}	4.10×10^{5}	4.45×10^{5}	5.34×10^{5}	3.23×10^{5}	2.13×10^{5}	2.19×10^{5}	2.26×10^{5}

© 2026 The Author(s). Published by the Royal Society of Chemistry

Table 2 Alignment ratio $\eta = \beta_{vec}/\beta_{tot}$ for all sixteen structures. ‡ marks $\Gamma = 0$ near-resonance-unstable 2P symmetric-closed cells

	Static				1P (Pockels)				2P (SHG)			
Molecule	Gas	ACN	NP	DCE	Gas	ACN	NP	DCE	Gas	ACN	NP	DCE
D–D_{open}	−1.00	−1.00	−1.00	−1.00	−1.00	−1.00	−1.00	−1.00	−1.00	−1.00	−1.00	−1.00
D–D_{closed}	−1.00	−1.00	−1.00	−1.00	−1.00	−1.00	−1.00	−1.00	+0.99‡	+0.86‡	+0.83‡	+0.86‡
A–A_{open}	+1.00	+1.00	+1.00	+1.00	+1.00	+1.00	+1.00	+1.00	+1.00	+1.00	+1.00	+1.00
A–A_{closed}	+1.00	+1.00	+1.00	+1.00	+1.00	+1.00	+1.00	+1.00	+0.86‡	−0.61‡	−0.51‡	−0.28‡
D–A_{open}	+0.90	+0.86	+0.86	+0.87	+0.90	+0.87	+0.87	+0.87	−0.86	+0.87	+0.87	+0.88
D–A_{closed}	+0.48	+0.77	+0.77	+0.76	+0.53	+0.77	+0.77	+0.77	+0.40	−0.88	−0.89	−0.93
D*y*–*y*D_{open}	−1.00	−1.00	−1.00	−1.00	−1.00	−1.00	−1.00	−1.00	−1.00	−1.00	−1.00	−1.00
D*y*–*y*D_{closed}	−1.00	−1.00	−1.00	−1.00	−1.00	−1.00	−1.00	−1.00	+0.86‡	−0.97‡	−0.97‡	−0.97‡
A*y*–*y*A_{open}	+1.00	+1.00	+1.00	+1.00	+1.00	+1.00	+1.00	+1.00	+1.00	+1.00	+1.00	+1.00
A*y*–*y*A_{closed}	+1.00	+1.00	+1.00	+1.00	+1.00	+1.00	+1.00	+1.00	+0.98‡	+0.71‡	+0.79‡	+0.90‡
D*y*–*y*A_{open}	+0.94	+0.91	+0.91	+0.91	+0.94	+0.91	+0.91	+0.92	+0.15	+0.91	+0.92	+0.92
D*y*–*y*A_{closed}	+0.79	+0.83	+0.83	+0.84	+0.81	+0.83	+0.84	+0.84	+0.65	−0.95	−0.96	−0.97
D*y*–A_{open}	+0.89	+0.84	+0.84	+0.85	+0.90	+0.84	+0.85	+0.85	−0.29	+0.85	+0.85	+0.86
D*y*–A_{closed}	+0.52	+0.79	+0.79	+0.79	+0.53	+0.79	+0.79	+0.80	+0.41	−1.00	−0.99	−0.83
D–*y*A_{open}	+0.95	+0.94	+0.94	+0.94	+0.95	+0.94	+0.94	+0.94	+0.96	+0.95	+0.95	+0.95
D–*y*A_{closed}	+0.78	+0.84	+0.84	+0.85	+0.79	+0.84	+0.85	+0.86	+0.66	−0.86	−0.87	−0.87

solvent values are blue-shifted. This comparison is used only to check the calculated excitation-energy range and is not taken as direct experimental validation of β.

3.2 Static responses

In the static limit (*cf.* Table 1), the gas-phase β_{tot}^{S} spans from $\sim 1.6 \times 10^3$ a.u. for symmetric A–A_{open} to 3.11×10^5 a.u. for the doubly extended push–pull D*y*–*y*A_{closed}. The symmetric D–D and A–A scaffolds give modest open-form responses ($\sim 10^3$ a.u.) that grow about fivefold on ring closure but stay well below the push–pull values. Alkyne extension within the symmetric scaffolds (D*y*–*y*D, A*y*–*y*A) raises the closed-form response somewhat without changing the picture: with no donor–acceptor asymmetry, η stays at $\pm$ 1 (*cf.* Table 2) and the absolute response remains small.

The large enhancements appear only when extended conjugation is combined with donor–acceptor asymmetry. The simple D–A scaffold already has an elevated open-form response of 2.34×10^4 a.u., almost an order of magnitude above the symmetric analogues. Ring closure adds about 93% to this in the gas phase ($2.34 \times 10^4 \rightarrow 4.52 \times 10^4$ a.u.) but drops η from 0.90 to 0.48, a sign that competing charge–transfer pathways spoil the vectorial alignment of the closed isomer.[19] Adding an alkyne on either side (D*y*–A and D–*y*A) raises the closed-form response further, to 1.45×10^5 and 1.43×10^5 a.u. Extending both sides at once while keeping the donor–acceptor asymmetry (D*y*–*y*A) gives the largest off-resonant value in the set, 3.11×10^5 a.u., about 16× that of D*y*–*y*D_{closed} and 15× that of A*y*–*y*A_{closed}. The push–pull asymmetry is what couples the extended conjugation into a coherent end-to-end polarization.[12,50] Ring closure and a longer π-system do not achieve this on their own. Anderson *et al.*[28] reported that although the push–pull substitution pattern showed no clear impact on the absorption maximum of the open DTEs, this led to significantly red-shift the absorption maximum of the closed DTE. They attributed the more than 100 nm bathochromic shift in absorption maximum of the closed D–A vis-ŕ-vis its D–D and A–A analogues to the ICT between the electron-donating julolidine arm and the electron-accepting *N*-methylpyridinium arm. The significantly higher β_{tot} of the closed forms of the studied chromophore also indicates superior ICT in the former than that in the latter.

The solvent effect on the static β_{tot} depends on molecular architecture (*cf.* Table 1). D–A_{open} decreases from 2.34×10^4 a.u. in the gas phase to about 1.62×10^4 a.u. in the three solvents. For D–A_{closed}, the solvent values are 2.54–2.62 × 10^5 a.u. and follow DCE > NP > ACN. The other push–pull open forms also decrease in solution. D*y*–A_{closed} and D–*y*A_{closed} are strongly enhanced, while D*y*–*y*A_{closed} stays close to its gas-phase value. Thus, the solvent response does not follow a single trend with dielectric constant. The largest static solution values are found for the closed push–pull derivatives, about 2.5–3.1 × 10^5 a.u. For D–A_{closed} and D*y*–A_{closed}, η increases from 0.48 and 0.52 in the gas phase to about 0.77 and 0.79 in solution, respectively (Table 2). The static NLO data are given in Tables S1–S4. Fig. 6a shows $\beta_{tot}^{closed}/\beta_{tot}^{open}$. The ratio is greater than unity for all eight architectures in the gas phase and in each continuum solvent, although the size of the increase varies among the structures. The aspects of $\beta_{tot}^{closed}/\beta_{tot}^{open}$ ratio are discussed elaborately in the following sections.

3.3 One-photon responses

At $\omega = 0.0428$ a.u., the Pockels response generally follows the "closed > open" ordering (Table 1, Fig. 6b). Gas-phase D–A is the exception: $\beta_{tot} = 5.59 \times 10^4$ a.u. for the open form and 4.90×10^4 a.u. for the closed form. In DCE, NP, and ACN, the closed-form D–A value is again higher than the open-form value. The symmetric scaffolds give small Pockels responses of order 10^3–10^4 a.u. Their response vectors stay aligned with the dipole ($|\eta| = 1$), as symmetry requires (*cf.* Table 2). In the gas phase the Pockels magnitude of D*y*–*y*A_{closed} reaches 1.38×10^6 a.u. with $\eta = 0.81$, so the response is both large and well directed. The largest solvent enhancement, however, belongs to D–A_{closed}, its magnitude

© 2026 The Author(s). Published by the Royal Society of Chemistry

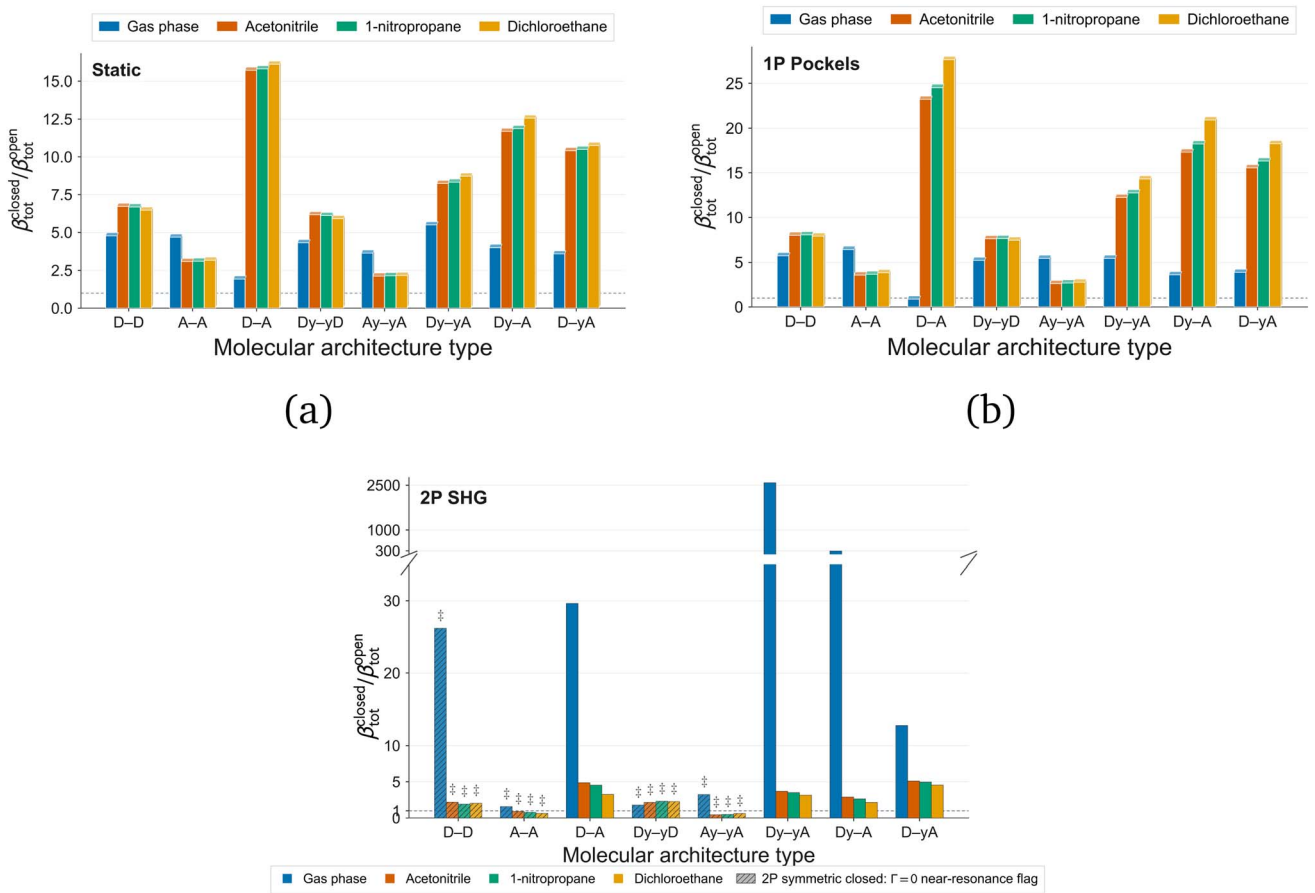


Fig. 6 Ring-closure enhancement of the total first hyperpolarizability, $\beta_{tot}^{closed}/\beta_{tot}^{open}$, across the eight chromophore architectures, four media, and three response regimes: (a) static, (b) 1P Pockels, and (c) 2P SHG. Panels (a) and (b) use linear ordinate scales; panel (c) uses a broken ordinate axis to accommodate the very large near-resonant gas-phase ratios; the dashed line marks unity. Hatched ‡ bars in the 2P panel identify symmetric closed-ring entries that are $\Gamma = 0$ near-resonance-unstable and should be read as ranking indicators rather than finite-linewidth observables. The ratios use the scalar magnitude β_{tot} only and should be interpreted together with the alignment ratio η (Table 2).

climbs nearly tenfold, from 4.90×10^4 a.u. in the gas phase to 4.66×10^5 a.u. in DCE. The alkyne-extended Dy–A_{closed}, by comparison, gains only about 1.5-fold over the same change ($3.76 \times 10^5 \rightarrow 5.50 \times 10^5$ a.u., gas to DCE). The solvent environment also significantly improves the alignment between the hyperpolarizability vector and the molecular dipole moment. For example, D–A_{closed} exhibits an increase in η from 0.53 in the gas phase to 0.77 in solution (*cf.* Table 2), while Dy–A_{closed} shows a similar increase from 0.53 to 0.79–0.80. Such improvements indicate that solvation not only amplifies the magnitude of the Pockels response but also promotes a more unidirectional intramolecular charge-transfer process. The three solvents give similar frequency-dependent NLO responses, with no common ordering by dielectric constant. For several closed push–pull systems, DCE gives the larger response. The main change occurs between the gas phase and the continuum-solvent calculations; differences among DCE, NP, and ACN are smaller and depend on the molecular architecture. Detailed one-photon frequency-dependent NLO data are given in Tables S5–S8.

3.4 Two-photon responses

The 2P regime is the most sensitive to the proximity of optically allowed states, because 2ω at $\omega = 0.0428$ a.u. falls into the visible-region absorption manifold of these chromophores (Tables S9–S12, S15 and Fig. 6c). The 2P response inherits both the enhancement and the phase sensitivity of near-resonant denominators on an allowed transition.[51] In general, the 2P regime activates response channels that are weak or absent under 1P excitation. The first bright excited state of the symmetric closed-ring D–D and Dy–yD scaffolds lies close to the two-photon resonance energy ($E_{S_1} \approx 2\omega$) [see Table S17]. In the undamped response formalism, the frequency-dependent hyperpolarizability contains energy denominators of the form $(E_n - 2\omega)^{-1}$, which become small near resonance, leading to artificially enhanced and numerically unstable response values.[52] So their undamped 2P responses are not numerically stable,[53] they change by large factors between gas and solvent, and the symmetry-required $|\eta| = 1$ is not reliably recovered

© 2026 The Author(s). Published by the Royal Society of Chemistry

(flagged entries, Tables 1 and 2). We therefore do not assign quantitative ring-closure 2P gains to those symmetric scaffolds.

In contrast, the push–pull chromophores discussed below lie sufficiently far from resonance poles, particularly in the solvent media DCE, NP, and ACN, and therefore provide the most reliable basis for interpreting the two-photon (2P) response (Table S15). For DCE, NP, and ACN, the quantitative comparison includes all open-ring entries and the four push–pull closed forms D–A_{closed}, D*y*–*y*A_{closed}, D*y*–A_{closed}, and D–*y*A_{closed}. The four symmetric closed forms D–D_{closed}, A–A_{closed}, D*y*–*y*D_{closed}, and A*y*–*y*A_{closed} are ‡-flagged and are excluded from quantitative 2P comparisons under the zero-damping convention. The sign reversals of η observed between the gas phase and solution for the D–A_{closed}, D*y*–*y*A_{closed}, D*y*–A_{closed} and D–*y*A_{closed} scaffolds (Table 2) arise from the near-resonant phase behavior of the gas-phase response function rather than from any chemically induced switching event. Consequently, the magnitudes of β_{tot} remain useful for ranking molecular performance when considered together with η.

Among the investigated systems, D*y*–*y*A_{closed} and D–*y*A_{closed} exhibit the strongest 2P responses, with β_{tot} values of approximately ~2.1–2.3 × 10^5 a.u. that are closely reproduced across all three solvents, followed by D*y*–A_{closed} with β_{tot} ~1.0 × 10^5 a.u. In contrast, taking ACN as the solvent reference, the gas-phase β_{tot} values of D*y*–*y*A_{closed} and D*y*–A_{closed} are larger by factors of about 134 and 16.3, respectively. For D–*y*A_{closed}, the corresponding factor is about 1.5. These apparent enhancements are dominated by undamped near-pole contributions in the sum-over-states expression and should not be interpreted as genuine physical improvements in nonlinear optical performance.

The TDDFT calculations directly support this interpretation. In the gas phase, each of these two chromophores possesses a dipole-allowed excited state (S_2) within 0.1 eV of the two-photon excitation energy, 2ω = 2.33 eV (D*y*–*y*A_{closed}, S_2 at 2.33 eV; D*y*–A_{closed}, S_2 at

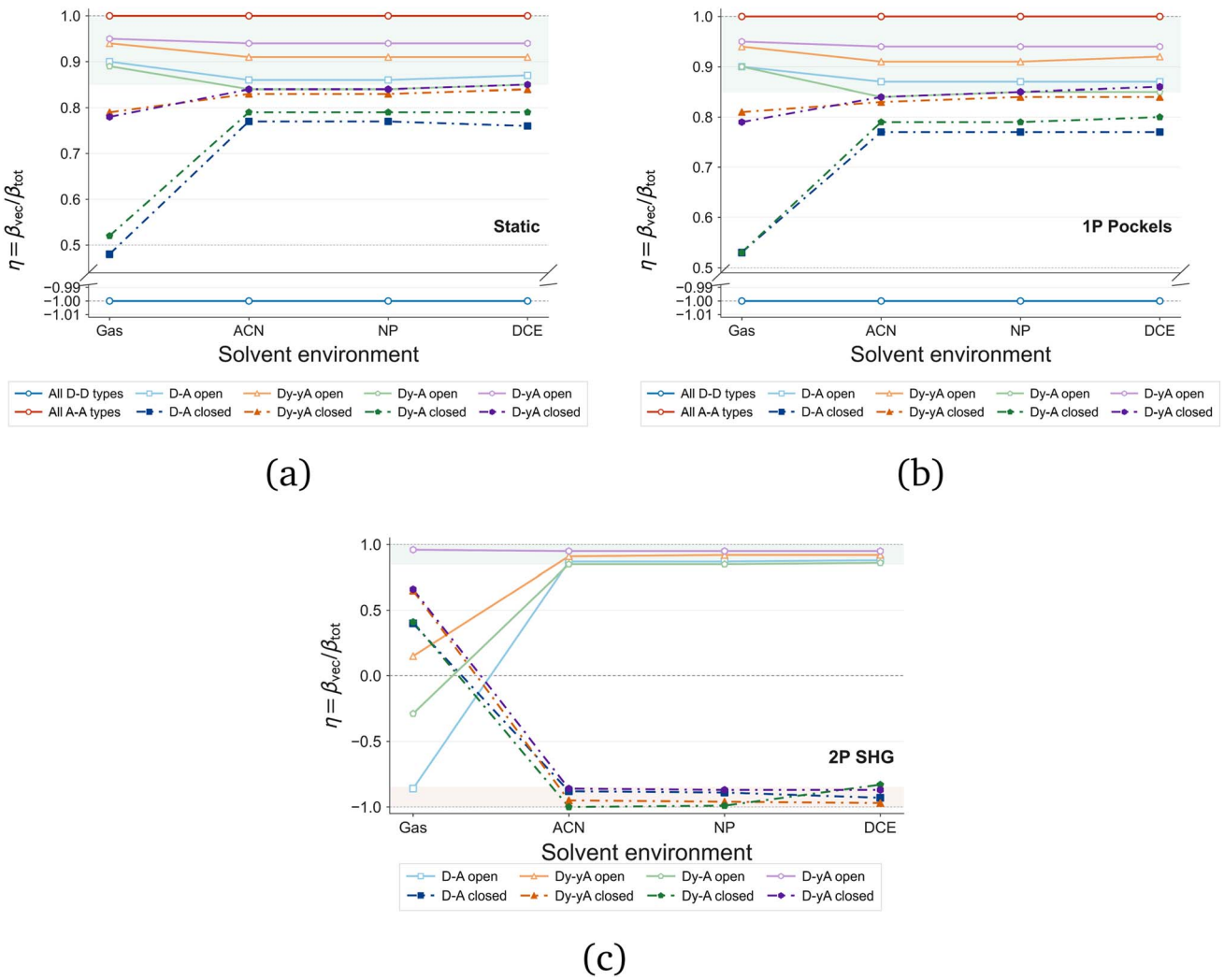


Fig. 7 Solvent-dependent alignment ratio $\eta = \beta_{vec}/\beta_{tot}$ across donor–acceptor architectures in the (a) static, (b) 1P Pockels, and (c) 2P SHG regimes. Panels (a) and (b) use expanded positive-η axes to resolve the static and Pockels trends; panel (c) uses the full signed range to show the 2P phase reversals. Solid traces with open markers denote open-ring forms; dash-dot traces with filled markers denote closed-ring forms. The pale green and red bands mark $|\eta| \geq 0.85$ positive and negative near-collinearity, respectively. The 2P panel makes the phase-sensitive sign changes explicit and shows the solvent-induced alignment of D*y*–*y*A_{open}.

© 2026 The Author(s). Published by the Royal Society of Chemistry

2.42 eV; Table S15). By contrast, D–A_{closed} and D–*y*A_{closed}, whose gas-phase β_{tot} values remain within a factor of three of their solvent-phase values, do not exhibit any dipole-allowed state within 0.1 eV of 2ω. Their nearest allowed transitions are located approximately 0.3–0.4 eV away. Solvation shifts the relevant excited states of all push–pull chromophores away from 2ω, thereby removing the near-resonant enhancement. As a result, the 2P responses of all four closed push–pull systems converge to values on the order of 10^5 a.u. in solution. The remaining gas-phase 2P magnitudes, including that of D–A_{closed}, differ from their solvent-phase counterparts by less than a factor of three and can therefore be regarded as physically meaningful manifestations of normal frequency-dispersion effects rather than resonance artifacts.

3.5 Solvent control of response magnitude and directionality

The static, 1P, and 2P trends above already make clear that solvent effects do not scale simply with the dielectric constant. This is consistent with the well-documented divergence between static and dynamic solvent responses for push–pull chromophores,[32,54,55] and with the more general finding that a dielectric medium can reorganize a chromophore's frontier orbitals rather than simply scale its response.[56] Two structure-dependent patterns of magnitude are already visible in the static closed/open ratios (Fig. 6a), and the same qualitative solvent sensitivity carries into the 1P tables (Fig. 6b). For symmetric D–D and D*y*–*y*D scaffolds, continuum solvation enhances β_{tot}^{S} but keeps $\eta = \pm 1$ unchanged. This indicates that solvation strengthens the nonlinear optical response without altering its direction. This feature can be seen from the bottom blue straight line with circles in the η plot shown in Fig. 7a and b. In contrast the symmetric A–A and A*y*–*y*A scaffolds exhibit the opposite behavior, continuum solvation decreases β_{tot}^{S} without affecting η (see top most magenta line in Fig. 7a and b). For the push–pull scaffolds, the open and closed isomers exhibit opposite solvent responses. The static and one-photon (1P) nonlinear optical responses of the open forms generally decrease in a polar dielectric medium (*cf.* Table 1), whereas those of the closed forms increase substantially. In the static regime, the closed/open response ratio in solution is ~16 for D–A, ~12 for D*y*–A, ~10–11 for D–*y*A, and ~8–9 for D*y*–*y*A (*cf.* Table 2). This behavior is consistent with the electron-density difference analysis, which shows that dielectric stabilization preferentially reinforces the closed-form geometry possessing a continuous donor-to-acceptor polarization pathway, while suppressing the response of the open forms that depend on a less coherent, multi-segment charge-transfer pathway.

The most distinctive solvent effect in the series is observed for D*y*–*y*A_{open} in the two-photon regime, where the solvent alters not only the magnitude but also the direction of the nonlinear optical response. In the gas phase, D*y*–*y*A_{open} exhibits a moderate 2P hyperpolarizability ($\beta_{tot} = 1.09 \times 10^4$ a.u.) and only a small fraction of this response is aligned with the molecular dipole ($\eta = 0.15$). The response is dominated by a transverse β_x contribution (*cf.* Table S9) and projects only weakly along the dipole axis. Upon solvation, the 2P response magnitude increases by approximately five- to sixfold, reaching $\sim 6 \times 10^4$ a.u. (*cf.* Fig. 6c), while the response vector undergoes a pronounced reorientation toward

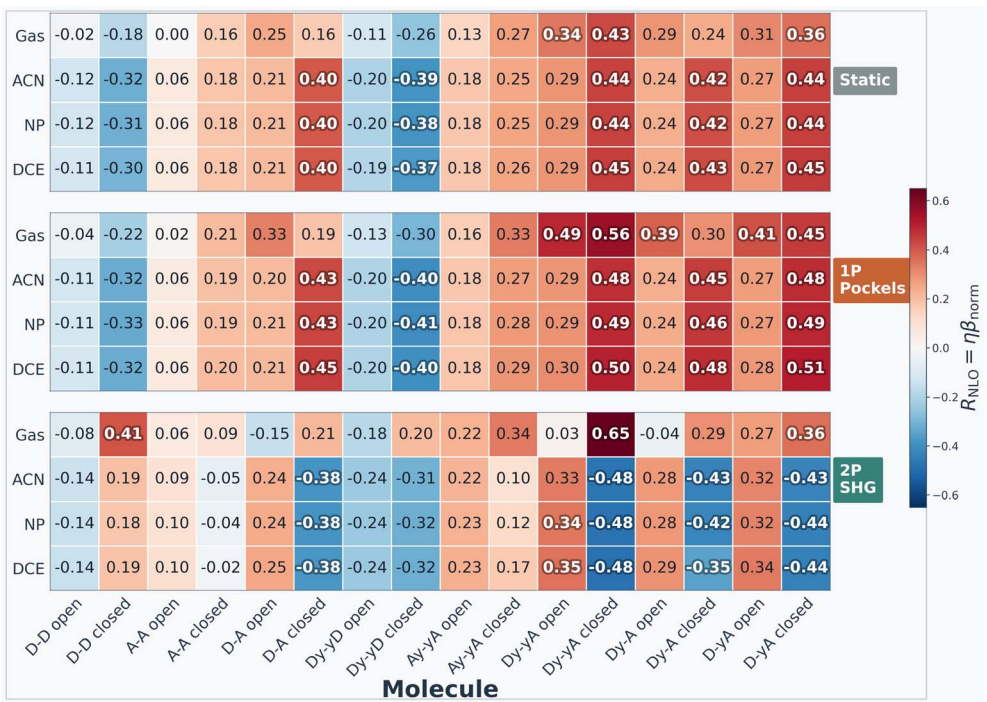


Fig. 8 Heatmap of the signed normalized descriptor $R_{NLO} = \beta_{norm}\eta$ across the 16 structures (eight motifs in their open and closed isomers), four media, and three response regimes (static, 1P Pockels, 2P SHG). β_{norm} is computed from the global logarithmic range of β_{tot} values used in the plot. The sign reports the direction of the response vector relative to the molecular dipole.

© 2026 The Author(s). Published by the Royal Society of Chemistry

the dipole direction (*cf.* orange line in Fig. 7c). Consequently, η rises dramatically to approximately 0.92 in all solvent environments considered. Thus, changing the solvent alone transforms the 2P response from being largely transverse to becoming strongly dipole-aligned. This behavior is unique to D*y*–*y*A_{open} among the chromophores studied. By contrast, the sign reversals of η observed for several other systems in Tables S9–S12 do not indicate a comparable physical reorientation of the response vector.

Overall, Fig. 7 reports the solvent-dependent alignment ratio, $\eta = \beta_{vec}/\beta_{tot}$, for the donor–acceptor architectures in the static, 1P, and 2P regimes. This figure separates molecules with genuinely directional response from those whose large tensor components partly cancel. In the static and 1P regimes the push–pull systems fall between $|\eta| = 0.5$ and 0.97 and become more dipole-aligned in solvent. In the 2P regime the alignment becomes strongly phase sensitive: open-form D*y*–*y*A rotates from weak gas-phase projection to positive solvent alignment, whereas several closed forms switch to negative η in solvent.

3.6 Combined magnitude and directional nonlinear responses

It is evident from the above discussion that a meaningful structure–property relationship for the NLO properties of the investigated chromophores cannot be established using either β_{tot} or η, alone. This is because these two descriptors characterize fundamentally different aspects of the NLO response and are not linearly correlated. Specifically, β_{tot} quantifies the magnitude of the first hyperpolarizability, whereas η characterizes the directional alignment of the contracted hyperpolarizability vector with the permanent molecular dipole moment. Thus, consideration of either descriptor independently provides only a partial description of the overall NLO response. A more comprehensive descriptor should therefore account simultaneously for both the magnitude and directional character of the response. To address this limitation, we introduced the combined descriptor R_{NLO}, defined in eqn (7), which incorporates both β_{tot} and η. The corresponding R_{NLO} values are represented as a heatmap in Fig. 8. In contrast to the trends obtained from β_{tot} or η individually, the combined descriptor provides a more balanced measure of the overall NLO performance. The heatmap reveals that the closed push–pull architectures exhibit the highest combined responses, with D*y*–*y*A_{closed}, D–*y*A_{closed}, and D*y*–A_{closed} emerging as the most favorable structures among the considered molecular scaffolds. This behavior demonstrates that a large hyperpolarizability magnitude alone does not necessarily translate into a strong overall NLO response when the response is poorly aligned. Conversely, the symmetric architectures, D–D, A–A, and D*y*–*y*D, generally exhibit smaller R_{NLO} values despite their relatively favorable alignment ratios. This arises because the beneficial contribution from $|\eta|$ is multiplied by a comparatively small NLO response magnitude. Thus, the combined descriptor successfully differentiates systems that may appear favorable when either magnitude or directional alignment is considered independently.

4 Conclusions

The purpose of this study is to reveal how ring topology, donor–acceptor architectures, π-extension, and dielectric environment reorganize the response tensor across a controlled chromophore family. Within the CAM-B3LYP/6-31+G(d,p)/GD3BJ/(PCM) framework adopted here, the NLO response is governed not by any single structural modification but by the interplay between the magnitude and direction of the hyperpolarizability tensor. The first hyperpolarizability of eight dithienylethene-based chromophores, comprising electronic donor/acceptor motifs with and without an alkyne extension, was investigated quantum chemically in both their open- and closed-ring forms in the gas phase and three solvent media (ACN, NP and DCE). The dynamic responses of β were studied at 1064 nm excitation wavelength. In the studied chromophores the β response behaves as a tensor whose magnitude, direction, and phase depend together on ring-isomer state, donor–acceptor asymmetry, π-extension, and dielectric environment. Ring closure restores through-core conjugation and generally increases β_{tot}, but the enhancement of the magnitude is dominantly dictated by the molecular topology, not by ring closure alone. Donor–acceptor asymmetry gives the largest responses by creating polar charge-transfer pathways, while symmetric closed scaffolds gain magnitude with $\eta \rightarrow \pm 1$ but remain weak, whereas push–pull closed scaffolds gain both magnitude and directionality. Alkyne (π-) extension is most effective when paired with donor–acceptor asymmetry. The doubly extended push–pull D*y*–*y*A_{closed} scaffold gives the largest gas-phase static and 1P responses, while the responses of the solvated extended push–pull systems are strongly medium dependent. Continuum solvation can amplify, attenuate, or rotate the response vector. Amplification is clearest for D–A_{closed} in the 1P regime, where the response grows by nearly an order of magnitude from gas to DCE. Reorientation is clearest for D*y*–*y*A_{open} in the 2P regime, where the response vector turns from largely transverse to the molecular dipole ($\eta = 0.15$, gas) to dipole-aligned ($\eta \rightarrow +0.92$, solvent) within the continuum-solvent model, a reorientation unique to this scaffold in the present series. Sign reversals in near-resonant 2P responses, common across the push–pull family, reflect phase-sensitive tensor interference.

The R_{NLO} analysis demonstrates that neither β_{tot} nor η alone is sufficient to describe the overall NLO performance of the investigated chromophores, as response magnitude and directional alignment can vary independently. By combining these two characteristics, R_{NLO} provides a more balanced comparative measure of NLO behavior. The analysis identifies the closed push–pull architectures, particularly D*y*–*y*A_{closed}, D–*y*A_{closed}, and D*y*–A_{closed}, as the most favorable systems because they combine large hyperpolarizability with favorable directional character. In contrast, symmetric chromophores exhibit relatively high alignment but weaker overall responses, resulting in lower R_{NLO} values. Thus, the R_{NLO} analysis establishes that optimal NLO performance requires simultaneous enhancement of response magnitude and directionality, providing a useful framework for

© 2026 The Author(s). Published by the Royal Society of Chemistry

rationalizing structure–property relationships across the investigated chromophore family. Overall present R_{NLO} analyses indicate that the ring closure and π-extension do not universally increase β. Our analysis showed that a large NLO response requires the scalar tensor norm and the response-vector direction to be optimized together. The donor–acceptor asymmetry sets the polarity, ring closure restores conjugation through the core, π-extension lengthens the polarizable path, and the dielectric environment reinforces or redirects the result in the studied DTE chromophores.

Author contributions

R. M. conceived the idea. K. S. and R. S. designed the study, performed the calculations, analyzed the data, and wrote the first draft of the manuscript. R. M. contributed to the interpretation of the results and to the manuscript writing. A. G. contributed to the chemical-physics framing and supervised the work at Ulm. All authors discussed the results and contributed to the final manuscript.

Conflicts of interest

The authors declare no competing financial interest.

Data availability

All data related to this study are provided in the main manuscript and the supporting information (SI). The geometries of the optimized structures are available from the corresponding authors upon reasonable request. Supplementary information: notes, complete tensor data for the static, one-photon (1P), and two-photon (2P) NLO responses, frontier orbital energies, excitation energies and corresponding oscillator strengths, and reproducibility data for β_{tot} and η obtained using the aug-cc-pVDZ basis set. See DOI: https://doi.org/10.1039/d6ra08114b.

Acknowledgements

R. M. thanks Prof. P. Hegemann for constant encouragement and acknowledges support from the Humboldt-Universität zu Berlin. K. S. and A. G. acknowledge support from the state of Baden-Württemberg through bwHPC and from the German Research Foundation (DFG) through grant INST 40/575-1 FUGG (bwForCluster JUSTUS 2), where the density-functional-theory calculations reported in this work were performed. Additional support from the Dr Barbara Mez-Starck Foundation is gratefully acknowledged. R.S. acknowledges financial support from the GITAM New SEED Grant [F. No. 2025/0004] and computational resources provided by GITAM's HPC facility, G-Cluster, and the Computational Research Laboratory (CRL), GITAM, Hyderabad.

Notes and references

1 A. Boes, L. Chang, C. Langrock, M. Yu, M. Zhang, Q. Lin, M. Lončar, M. Fejer, J. Bowers and A. Mitchell, *Science*, 2023, **379**, eabj4396.
2 F. Ullah, N. Deng and F. Qiu, *PhotoniX*, 2021, **2**, 13.
3 Y. Zhang, D. D. Xu, I. Tanriover, W. Zhou, Y. Li, R. López-Arteaga, K. Aydin and C. A. Mirkin, *Nat. Photonics*, 2025, **19**, 20–27.
4 M. S. Wong, C. Bosshard, F. Pan and P. Günter, *Adv. Mater.*, 1996, **8**, 677–680.
5 S. Semin, X. Li, Y. Duan and T. Rasing, *Adv. Opt. Mater.*, 2021, **9**, 2100327.
6 R. Gompper and H.-U. Wagner, *Angew Chem. Int. Ed. Engl.*, 1988, **27**, 1437–1455.
7 H. Wang, M. Mutailipu, Z. Yang, S. Pan and J. Li, *Angew. Chem., Int. Ed.*, 2025, **64**, e202420526.
8 A. Sen, M. H. Putra, A. K. Biswas, A. K. Behera and A. Groß, *Dyes Pigm.*, 2023, **213**, 111087.
9 T. Hrivnák, M. Medveď, W. Bartkowiak and R. Zaleśny, *Molecules*, 2022, **27**, 8738.
10 P. K. Samanta and R. Misra, *J. Appl. Phys.*, 2023, **133**, 020901.
11 G. Maroulis, *J. Chem. Phys.*, 1999, **111**, 583–591.
12 F. Bureš, *RSC Adv.*, 2014, **4**, 58826–58851.
13 A. Sen and A. Groß, *J. Phys. Chem. C*, 2020, **124**, 8526–8540.
14 Y. Siqueira, M. L. Lyra, T. N. Ramos, B. Champagne and V. Manzoni, *J. Chem. Phys.*, 2022, **156**, 014305.
15 D. Bléger and S. Hecht, *Angew. Chem., Int. Ed.*, 2015, **54**, 11338–11349.
16 W. R. Browne and B. L. Feringa, in *Molecular Switches*, ed. B. L. Feringa and W. R. Browne, Wiley-VCH, 2nd edn, 2011, pp. 121–179.
17 J.-X. Wang, C. Li and H. Tian, *Coord. Chem. Rev.*, 2021, **427**, 213579.
18 F. Castet, C. Tonnelé, L. Muccioli and B. Champagne, *Acc. Chem. Res.*, 2022, **55**, 3716–3726.
19 K. J. Chen, A. D. Laurent and D. Jacquemin, *J. Phys. Chem. C*, 2014, **118**, 4334–4345.
20 M. Irie, T. Fukaminato, T. Sasaki, N. Tamai and T. Kawai, *Nature*, 2002, **420**, 759–760.
21 Y. Arai, S. Ito, H. Fujita, Y. Yoneda, T. Kaji, S. Takei, R. Kashihara, M. Morimoto, M. Irie and H. Miyasaka, *Chem. Commun.*, 2017, **53**, 4066–4069.
22 W. A. Velema, W. Szymanski and B. L. Feringa, *J. Am. Chem. Soc.*, 2014, **136**, 2178–2191.
23 A. Perrier, S. Aloise, M. Olivucci and D. Jacquemin, *J. Phys. Chem. Lett.*, 2013, **4**, 2190–2196.
24 E. Kim, M. Kim and K. Kim, *Bull. Korean Chem. Soc.*, 2008, **29**, 827–832.
25 J. Jin, J. Zhang, L. Zou and H. Tian, *Analyst*, 2013, **138**, 1641–1644.
26 E. Kim, M. Kim and K. Kim, *Tetrahedron*, 2006, **62**, 6814–6821.
27 A. Sen and A. Groß, *ACS Appl. Energy Mater.*, 2019, **2**, 6341–6347.
28 S. Qiu, A. T. Frawley, K. G. Leslie and H. L. Anderson, *Chem. Sci.*, 2023, **14**, 9123–9135.
29 S. J. A. van Gisbergen, J. G. Snijders and E. J. Baerends, *J. Chem. Phys.*, 1998, **109**, 10644–10656.
30 S. Löffelsender, P. Beaujean and M. de Wergifosse, *Wiley Interdiscip. Rev.:Comput. Mol. Sci.*, 2024, **14**, e1695.

 © 2026 The Author(s). Published by the Royal Society of Chemistry

31 J. M. Herbert, *Wiley Interdiscip. Rev.:Comput. Mol. Sci.*, 2021, **11**, e1519.
32 S. Fonseca, N. S. S. dos Santos, A. R. da Cunha, S. Canuto, P. F. Provasi, T. Andrade-Filho and R. Gester, *ChemPhysChem*, 2023, **24**, e202300060.
33 T. Yanai, D. P. Tew and N. C. Handy, *Chem. Phys. Lett.*, 2004, **393**, 51–57.
34 J. E. Del Bene, W. B. Person and K. Szczepaniak, *J. Phys. Chem.*, 1995, **99**, 10705–10707.
35 P.-F. Loos, M. Comin, X. Blase and D. Jacquemin, *J. Chem. Theory Comput.*, 2021, **17**, 3666–3686.
36 M. S. Kodikara, R. Stranger and M. G. Humphrey, *ChemPhysChem*, 2018, **19**, 1537–1546.
37 B. Kirtman, S. Bonness, A. Ramirez-Solis, B. Champagne, H. Matsumoto and H. Sekino, *J. Chem. Phys.*, 2008, **128**, 114108.
38 E. Cancčs, B. Mennucci and J. Tomasi, *J. Chem. Phys.*, 1997, **107**, 3032–3041.
39 B. Mennucci, *Wiley Interdiscip. Rev.:Comput. Mol. Sci.*, 2012, **2**, 386–404.
40 M. J. Frisch, G. W. Trucks, H. B. Schlegel, G. E. Scuseria, M. A. Robb, J. R. Cheeseman, G. Scalmani, V. Barone, G. A. Petersson, H. Nakatsuji, X. Li, M. Caricato, A. V. Marenich, J. Bloino, B. G. Janesko, R. Gomperts, B. Mennucci, H. P. Hratchian, J. V. Ortiz, A. F. Izmaylov, J. L. Sonnenberg, D. Williams-Young, F. Ding, F. Lipparini, F. Egidi, J. Goings, B. Peng, A. Petrone, T. Henderson, D. Ranasinghe, V. G. Zakrzewski, J. Gao, N. Rega, G. Zheng, W. Liang, M. Hada, M. Ehara, K. Toyota, R. Fukuda, J. Hasegawa, M. Ishida, T. Nakajima, Y. Honda, O. Kitao, H. Nakai, T. Vreven, K. Throssell, J. A. Montgomery Jr, J. E. Peralta, F. Ogliaro, M. J. Bearpark, J. J. Heyd, E. N. Brothers, K. N. Kudin, V. N. Staroverov, T. A. Keith, R. Kobayashi, J. Normand, K. Raghavachari, A. P. Rendell, J. C. Burant, S. S. Iyengar, J. Tomasi, M. Cossi, J. M. Millam, M. Klene, C. Adamo, R. Cammi, J. W. Ochterski, R. L. Martin, K. Morokuma, O. Farkas, J. B. Foresman and D. J. Fox, *Gaussian 16 Revision C.01*, Gaussian Inc., Wallingford CT, 2016.
41 S. Grimme, S. Ehrlich and L. Goerigk, *J. Comput. Chem.*, 2011, **32**, 1456–1465.
42 S. K. Chaluvadi, S. Punathum Chalil, F. Mazzola, S. Dolabella, P. Rajak, M. Ferrara, R. Ciancio, J. Fujii, G. Panaccione, G. Rossi and P. Orgiani, *Sci. Rep.*, 2023, **13**, 3882.
43 R. Dennington, T. A. Keith and J. M. Millam, *GaussView Version 6*, Semichem Inc. Shawnee Mission KS, 2019.
44 D. A. Kleinman, *Phys. Rev.*, 1962, **126**, 1977–1979.
45 S. P. Karna and M. Dupuis, *J. Comput. Chem.*, 1991, **12**, 487–504.
46 A. K. Jeewandara and K. N. de Silva, *J. Mol. Struct.:THEOCHEM*, 2004, **686**, 131–136.
47 D. F. S. Machado, T. O. Lopes, I. T. Lima, D. A. da Silva Filho and H. C. B. de Oliveira, *J. Phys. Chem. C*, 2016, **120**, 17660–17669.
48 J. L. Oudar and D. S. Chemla, *J. Chem. Phys.*, 1977, **66**, 2664–2668.
49 A. Cesaretti, P. Foggi, C. G. Fortuna, F. Elisei, A. Spalletti and B. Carlotti, *J. Phys. Chem. C*, 2020, **124**, 15739–15748.
50 A. Dutta, A. Iglesias-Reguant, J. M. Luis, R. Misra and N. Deb, *J. Phys. Chem. A*, 2025, **129**, 5427–5437.
51 C. H. D. dos Santos, L. H. Zucolotto Cocca, A. G. Pelosi, V. F. Batista, D. C. G. A. Pinto, M. A. F. Faustino, M. G. Vivas, J. de Paula Siqueira, C. R. Mendonça and L. De Boni, *J. Chem. Phys.*, 2023, **158**, 214201.
52 X. Hu, D. Xiao, S. Keinan, I. Asselberghs, M. J. Therien, K. Clays, W. Yang and D. N. Beratan, *J. Phys. Chem. C*, 2010, **114**, 2349–2359.
53 P. Norman, *Phys. Chem. Chem. Phys.*, 2011, **13**, 20519–20535.
54 N. I. Shalin, Y. A. Phrolycheva, O. D. Fominykh and M. Y. Balakina, *J. Mol. Liq.*, 2021, **330**, 115665.
55 C. Bouquiaux, P. Beaujean, T. N. Ramos, F. Castet, V. Rodriguez and B. Champagne, *J. Chem. Phys.*, 2023, **159**, 174307.
56 M. H. Putra, B. Bagemihl, S. Rau and A. Groß, *Chem. – Eur. J.*, 2024, **30**, e202302643.

© 2026 The Author(s). Published by the Royal Society of Chemistry